

Ice shelf density reconstructed from optical televiewer borehole logging

Bryn Hubbard,¹ Jean-Louis Tison,² Morgane Philippe,² Billie Heene,² Frank Pattyn,² Terry Malone,¹ and Johannes Freitag³

Received 17 September 2013; revised 23 October 2013; accepted 28 October 2013; published 19 November 2013.

[1] Optical televiewer luminosity logs are compared with densities measured gravimetrically on 520 snow, firn, and ice samples from two locations of similar annual temperature ($\sim -14^{\circ}\text{C}$) and contrasting accumulation rates (0.23 and 0.43 m water equivalent per year) on the Roi Baudouin Ice Shelf, Antarctica. At the scale of $\geq 10^{-1}$ m, an inverse exponential relationship ($R^2=0.96$) is recorded between density and luminosity, indicating (i) that optical televiewing luminosity provides an effective proxy for density at such ice shelves and (ii) that densities may be reconstructed from boreholes drilled elsewhere by hot water without the need for core material. Our analysis also suggests that this relationship may hold for newly formed ice as well as for snow and firn. At the scale of $\leq 10^{-1}$ m, both luminosity and density show similar patterns, but precise correlation is confounded by detailed differences between the two records. **Citation:** Hubbard, B., J.-L. Tison, M. Philippe, B. Heene, F. Pattyn, T. Malone, and J. Freitag (2013), Ice shelf density reconstructed from optical televiewer borehole logging, *Geophys. Res. Lett.*, 40, 5882–5887, doi:10.1002/2013GL058023.

1. Introduction

[2] Ice mass firnification involves the progressive close off of air passages as snow densifies from an aggregate of individual flakes, through firn, characterized by interconnected air passages, to glacier ice, where gas is occluded as bubbles. As ice is buried, it experiences a corresponding increase in pressure that collapses the bubbles, and gas is eventually held in the form of clathrates, creating clear, bubble-free ice below depths of approaching 1 km [e.g., Gerland *et al.*, 1999]. These processes of firnification and burial are closely associated with progressive densification, increasing from $\sim 300 \text{ kg m}^{-3}$ for fresh snow, through $\sim 830 \text{ kg m}^{-3}$ for newly formed ice, to $\sim 910 \text{ kg m}^{-3}$ for deep, bubble-free ice. Since this densification is closely associated with a reduction in the quantity of reflective crystal boundaries and gas inclusions, the bulk optical reflectivity of the snow, firn and ice involved also generally decreases with firnification and depth. The surface materials of an ice mass thereby progress from highly reflective snow (with an albedo of ~ 0.8), through intermediate firn, to bubble-rich ice (with an albedo of ~ 0.4 – 0.3), and

eventually to bubble-free ice that may be virtually transparent. One exception to this general trend has been reported in the uppermost ~ 10 m of accumulating snow or up to a density of $\sim 550 \text{ kg m}^{-3}$. Here, initial densification occurs predominantly through settling by grain boundary sliding [e.g., Alley *et al.*, 1987] which increases scattering area per unit volume, causing reflectance to increase with density and therefore depth. This effect has been recorded directly by both core imaging and near-surface borehole optical logging [e.g., Hawley and Morris, 2006; Hubbard and Malone, 2013]. Below this, densification becomes dominated by sintering and scattering generally decreases with continued firnification.

[3] The precise association between light transmittance and the density of snow, firn and ice is complex, involving a small amount of absorption, which is generally neglected, and the influence of various scatterers, dominated by the presence of air-ice surfaces in snow and firn and by the presence of bubbles and other inclusions in ice. Although constrained to different degrees [Fudge and Smith, 2010], investigations of ice cores [e.g., Breton *et al.*, 2009; Sjögren *et al.*, 2007] indicates that these properties combine together such that light transmittance generally scales with density through firnification and subsequent ice compaction. Although extremely valuable, optical analysis of core material depends both on a sufficiently long ice core being available, itself a major logistical undertaking, and on the absence of scatterers unrelated to density within the ice samples available. Both of these limitations can potentially be overcome by continuous measurements of the reflectance of the walls of boreholes drilled into ice masses, which can be cored or drilled more rapidly by hot water. A few studies have applied this borehole-based approach using, for example, gamma scattering [Gerland *et al.*, 1999], neutron scattering [Hawley and Morris, 2006; Morris and Cooper, 2003], laser scattering [Bramall *et al.*, 2005], as well as optical video. Hawley and Morris [2006] applied the last of these to compare the luminosity of directional borehole video with neutron probe measurements, a surrogate for snow and firn density, over a ~ 30 m long borehole drilled at Summit, Greenland. This study revealed that the optical log provided a good proxy for the neutron-derived density, yielding a generally positive correlation between light intensity and density in the uppermost ~ 15 m of the borehole and a generally negative correlation below that. However, despite this general agreement (and the use of low-pass filtering), detailed comparison between the two records was variable: Correlation coefficients calculated for discrete 2.5 m long windows had values that fell from a peak of 0.854 in the depth range 7.5–10.0 m to a minimum of -0.012 in the depth range 20.0–22.5 m.

[4] Digital optical televiewing (OPTV) yields a geometrically accurate optical image of the complete wall of any logged borehole. It thereby provides a more tightly constrained and complete record of borehole luminosity than

¹Centre for Glaciology, Institute of Geography and Earth Sciences, Aberystwyth University, Aberystwyth, UK.

²Laboratoire de Glaciologie, Département des Sciences de la Terre et de l'Environnement, Université Libre de Bruxelles, Brussels, Belgium.

³Alfred Wegener Institute, Bremerhaven, Germany.

Corresponding author: B. Hubbard, Centre for Glaciology, Institute of Geography and Earth Sciences, Aberystwyth University, Llandinam Bldg., Aberystwyth SY23 3DB, UK. (byh@aber.ac.uk)

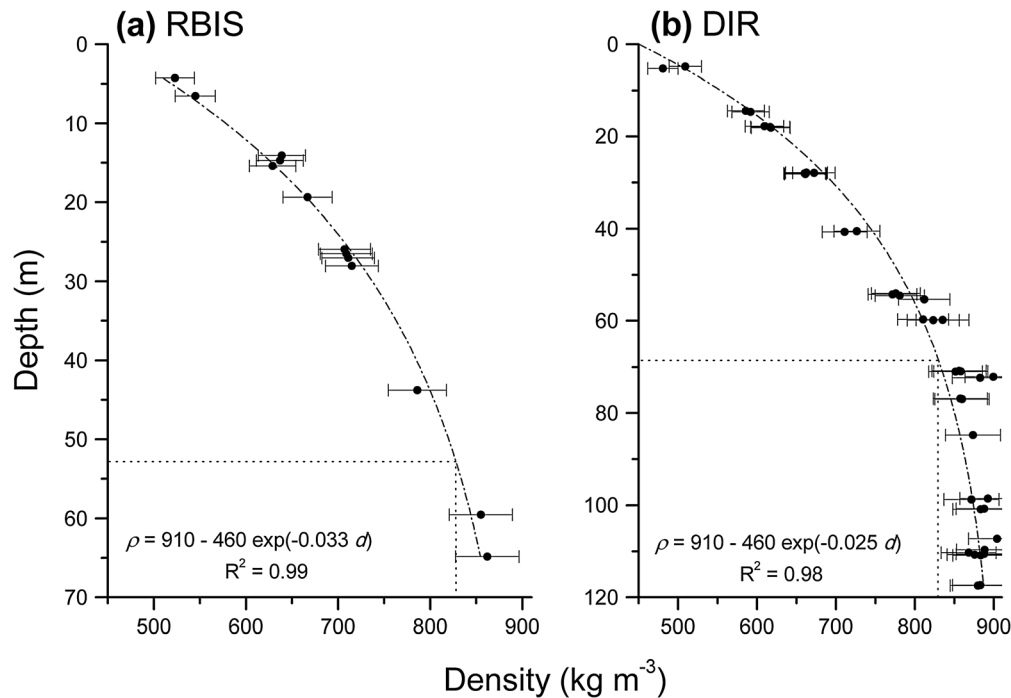


Figure 1. Density measured gravimetrically on core samples plotted against depth for (a) the RBIS core and (b) the DIR core. The $\pm 4\%$ bars reflect measured, at-a-depth variation. Dashed line and equation give best fit exponential relationship between the variables. Dotted lines indicate the location of the firm-ice transition, defined by a density of 830 kg m^{-3} ($\sim 53 \text{ m}$ at RBIS and $\sim 70 \text{ m}$ at DIR). Note the different depth scales.

does directional video [e.g., Hubbard *et al.*, 2008]. In this paper we evaluate the ability of OPTV luminosity to act as a proxy for snow, firn, and ice density by comparing OPTV logs of two boreholes drilled in the area of the Roi Baudouin Ice Shelf, Antarctica, with densities measured by gravimetry on core segments recovered from those boreholes.

2. Field Site and Methods

2.1. Field Site

[5] The Roi Baudouin Ice Shelf is located at $\sim 70^\circ\text{S}$, $\sim 24^\circ\text{E}$ on the Princess Ragnhild Coast of East Antarctica. Two ice cores and associated boreholes are investigated herein. The first, Roi Baudouin Ice Shelf (RBIS), is located on the ice shelf, has a surface elevation of $\sim 50 \text{ m}$ above sea level (asl) and a mean annual temperature (measured on ice core sections from below 15 m depth) of -13.8°C . The second, Derwael Ice Rise (DIR), is located $\sim 70 \text{ km}$ to the east on the crest of the Derwael Ice Rise, has a surface elevation of $\sim 450 \text{ m}$ asl and a mean annual temperature of -13.7°C .

2.2. Methods

2.2.1. Borehole Drilling and OPTV Logging

[6] The two boreholes reported here were drilled by Eclipse electromechanical corer, yielding 82 mm diameter core. The RBIS borehole is $\sim 67 \text{ m}$ long and that at DIR is $\sim 118 \text{ m}$ long, and both are air filled. At RBIS, the uppermost $\sim 20 \text{ m}$ of snow and firn was sampled from a second borehole drilled adjacent to the main hole. Material density is not therefore compared with OPTV data at the scale of $< 10^{-1} \text{ m}$ over the uppermost 20 m of RBIS.

[7] Once cores were recovered, boreholes were logged by OPTV at a resolution of $\sim 1 \text{ mm}$ laterally and vertically. The

OPTV probe used here emits light from a radial array of 72 light-emitting diodes (LEDs). Having intersected the borehole wall, the proportion of this light reflected back to the probe passes through a transparent cylindrical window and onto a hyperboloidal mirror located $\sim 0.08 \text{ m}$ below the LED array. The mirror is imaged from above by the probe's downward-looking camera, which thereby records the entire circumference of the adjacent borehole wall as a ring of pixels (further details are provided by Hubbard *et al.* [2008]). The resulting OPTV logs were analyzed and presented as rectangular images orientated to progress N-E-S-W-N from left to right using WellCADTM software. The nondimensional luminosity measured by the OPTV probe's camera was calculated over the range 0–255 as the mean of each lateral pixel ring using Borehole and Ice Feature Annotation Tool software [Malone *et al.*, 2013].

2.2.2. Density Measurements

[8] Once drilled, ice core sections were logged in the field and thereafter stored at $\sim -22^\circ\text{C}$ during transport back to the laboratory. Material density was measured by gravimetry in a cold room at -15°C . Four hundred seventy-two cubes of dimension $\sim 26 \text{ mm}$ were cut and analyzed from 13 core sections from RBIS, and 48 square columnar core sections, each of 28 mm wide and $0.05\text{--}0.25 \text{ m}$ long, were cut and analyzed from DIR. Once cut, precise sample dimensions were measured 3 times in each direction by digital caliper to a precision of 0.02 mm . Each sample was weighed 3 times by analytical scale to a precision of 0.1 mg . Measurements were repeated on two different samples for each depth interval for the RBIS core, comparison of which yielded a standard deviation in measured density of $< 4\%$. Empirical comparison was not carried out for the DIR samples, which took up more of the available core, but their larger size gives

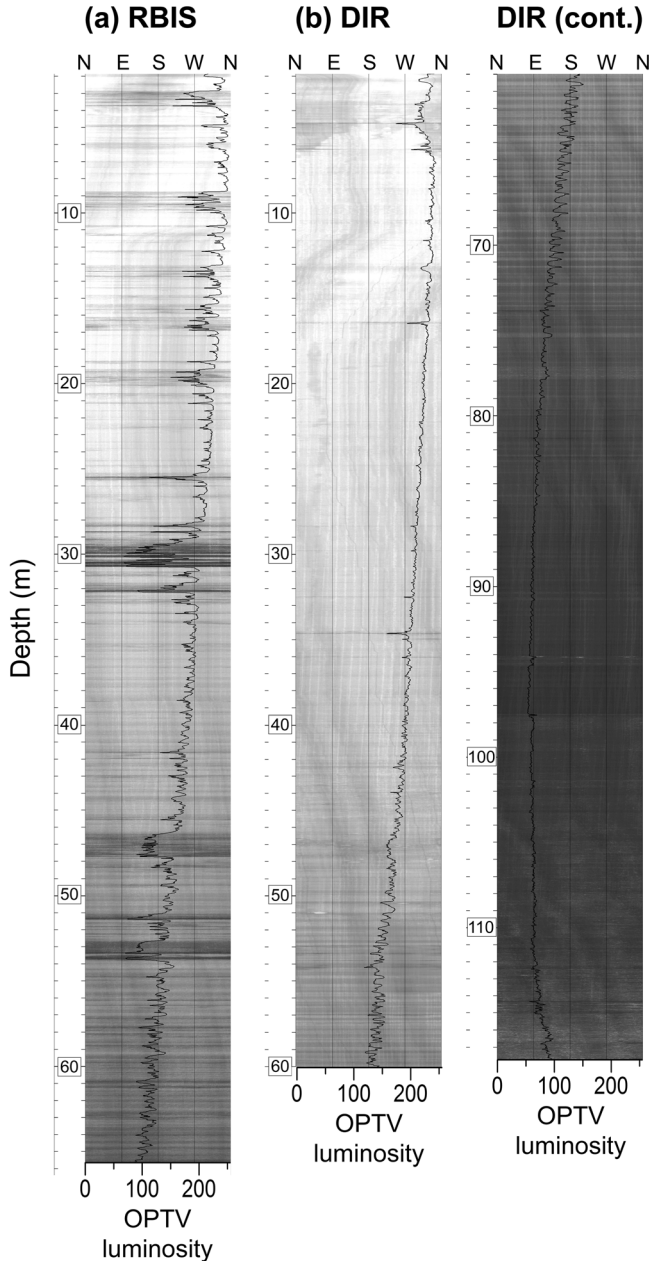


Figure 2. Raw OPTV logs with overlaid luminosity traces for (a) the RBIS borehole and (b) the DIR borehole, presented in two sections. Note that the quasi vertical streaks along the logs are caused by scoring of the borehole walls by corer and OPTV probe centralizers.

confidence that variation in measured density is less than that for the RBIS samples.

2.3. OPTV Luminosity and Core Density

2.3.1. Borehole-Scale Trend ($\geq 10^{-1}$ m)

[9] Gravimetric-measured density along the full RBIS core shows an increase in density with depth, rising from just under 500 kg m^{-3} at a depth of ~ 4 m below the surface to approaching 900 kg m^{-3} at the base of the core. Each core section analyzed is also characterised by small-scale layering, considered in section 2.3.2 below. For the purpose of analysis at the scale of $\geq 10^{-1}$ m, the mean density of each

core section sampled from the RBIS core is plotted against its centerpoint depth, yielding data of a similar scale to the DIR samples (section 2.2.2 above). The resulting profiles (Figure 1) show a steady increase in density with depth that may be fitted, following *Sjögren et al.* [2007], to an exponential function of the form

$$\rho(d) = \rho_{\text{ice}} - (\rho_{\text{ice}} - \rho_{\text{snow}}) e^{\alpha d} \quad (1)$$

where ρ is density (kg m^{-3}), d is depth below the surface (m), and α is determined empirically. The best fit of our gravimetric density measurements to this function, fixing ρ_{ice} at 910 kg m^{-3} and ρ_{snow} at 450 kg m^{-3} , gives $\alpha = -0.033$ ($R^2 = 0.99$; $\text{SE} = 6.9 \times 10^{-4}$) for RBIS (Figure 1a) and $\alpha = -0.025$ ($R^2 = 0.98$; $\text{SE} = 8.8 \times 10^{-4}$) for DIR (Figure 1b). These data indicate a more rapid increase in density with depth at RBIS than at DIR and that the firm-ice transition (830 kg m^{-3}) occurs at a depth of ~ 53 m at RBIS and at ~ 70 m at DIR.

[10] The complete OPTV logs of the RBIS and DIR boreholes are presented in Figure 2. Luminosity increases slightly over the uppermost few meters, with the maximum values of ~ 250 for each log located at a depth of 4.81 m at RBIS and 7.05 m at DIR. These are shallower than equivalent depths measured on the Greenland ice sheet (section 1), indicating that grain boundary sliding gives way to sintering sooner on the relatively warm Roi Baudouin Ice Shelf. Below this, luminosity generally decreases with depth, falling to values of < 100 at ~ 100 m in the DIR borehole. However, the OPTV log of this borehole also shows an anomalous increase in luminosity below this minimum, between the depths of ~ 100 m and its base at ~ 118 m (Figure 2b). We attribute this to a methodological artifact related to a marked slow down in the rate of coring in this zone. Here, the drill's cutting teeth advanced only very slowly, effectively skating on the base of the hole, and quite possibly scoring the edge of the borehole in a way that served to increase its reflectance artificially.

[11] To allow direct comparison between the OPTV luminosity data and the density data, we subsampled and averaged the OPTV luminosities over the same decimeter length core sections as those analyzed gravimetrically for density. All data were used except samples from depths below 100 m in the DIR borehole (where OPTV luminosity is influenced by coring) and those from above 4.81 m at RBIS and 7.05 m at DIR (where densification is dominated by grain boundary sliding). Plotting gravimetrically measured density (ρ) against OPTV luminosity (L) (Figure 3) reveals a very close match to an exponential relationship of the form

$$\rho = \rho_{\text{ice}} - \delta e^{\varepsilon L} \quad (2)$$

which yields best fit values of $\delta = 15.4$ and $\varepsilon = 0.013$ ($R^2 = 0.94$) for RBIS (Figure 3a) and $\delta = 17.6$ and $\varepsilon = 0.012$ ($R^2 = 0.97$) for DIR (Figure 3b).

[12] One key issue concerning the applicability of OPTV luminosity as a proxy for snow and ice density is whether a single calibration between the two variables holds universally or whether local calibration is needed for each borehole analyzed. Combining the data from both sites and fitting them to equation (2) (Figure 3c) yields best fit values of $\delta = 17.2$ and $\varepsilon = 0.012$ and an R^2 of 0.96. This suggests that a similar relationship between OPTV luminosity and density

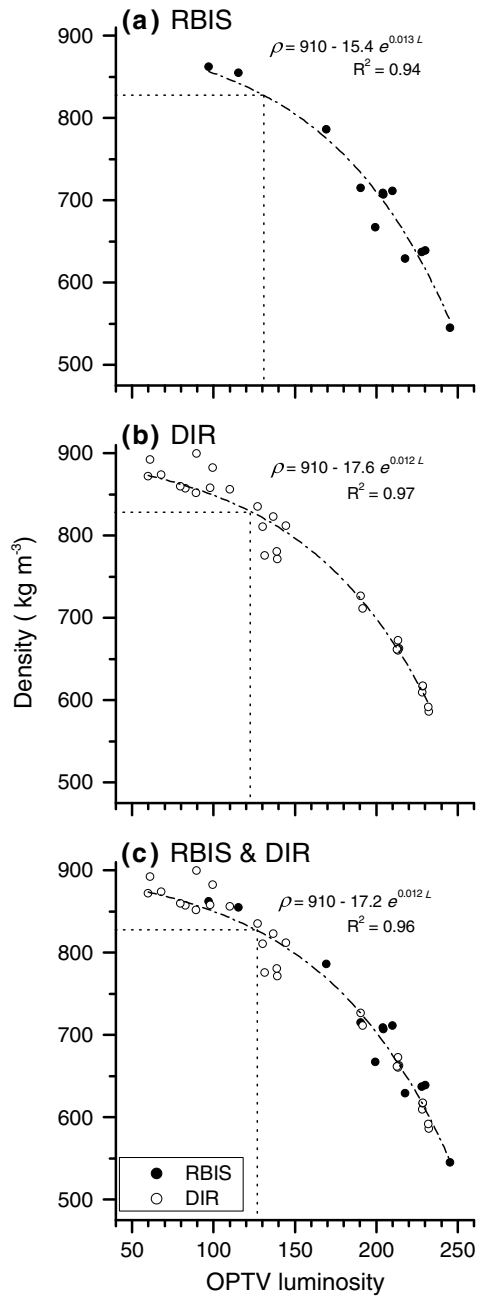


Figure 3. Gravimetrically measured density plotted against OPTV luminosity for (a) the RBIS borehole, (b) the DIR borehole, and (c) both boreholes combined. DIR readings from deeper than 100 m have been removed, as have RBIS data from shallower than 4.81 m and DIR data from shallower than 7.05 m (explained in the text).

holds for at least these two boreholes. It also allows the accumulation rate at both sites to be calculated solely from their OPTV logs. Associating OPTV-derived annual layer thicknesses (Figure 2) with densities reconstructed from equation (2) for both complete boreholes indicates mean accumulation rates of 0.23 and 0.43 m w.e. a⁻¹ at RBIS and DIR, respectively. This difference is consistent with the more rapid rate of densification with depth recorded at RBIS (Figure 1).

[13] The exponential relationship between density and luminosity appears to continue for the full lengths of both

boreholes, i.e., beyond the firm-ice transition. Applying equation (2) to the 13 samples with a density of >830 kg m⁻³ (i.e., those located in the upper left hand corner of Figure 3c) yields $\delta = 14.4$ and $\varepsilon = 0.012$ ($R^2 = 0.32$). Although less certain than for snow and firm, this analysis indicates that OPTV luminosity could also potentially provide a functional proxy for ice density.

2.3.2. Small-Scale Variations ($\leq 10^{-1}$ m)

[14] As noted in section 2.3.1, both borehole logs are characterized by the presence of regularly repeated light and dark bands (Figure 2). At this low-elevation ice shelf, located at $\sim 70^\circ\text{S}$, the darker layers are considered to form by a variable degree of melting each summer. As well as these regular annual layers, numerous thicker and generally darker bands also appear in both OPTV logs (Figure 2), likely to be caused by intense surface melting during the summer [Hubbard *et al.*, 2012].

[15] Excluding core from the uppermost ~ 20 m (section 2.2.1 above), 112 high-resolution gravimetrically measured density samples from seven sections of the RBIS core are available for direct comparison with OPTV luminosity. However, despite precise drill depths being recorded for each run, unavoidable errors occur as a result of, for example, core compression (particularly in snow and firm) and uneven core ends. Although we experienced no core loss, we estimate our drill depth error to be ≤ 0.1 m. Depths were therefore matched for each complete core subsection by correlating gravimetric density with OPTV luminosity for each 1 mm shift over a 0.1 m window either side of the logged depth and selecting the offset with the highest correlation coefficient. The resulting comparisons all reveal that the general trends are well matched between the two records, but that they deviate in detail. This comparison is illustrated by a sequence of four separate core sections between the depths of ~ 25.5 m and ~ 28.5 m (Figure 4). Here, the general decreases in luminosity at 25.65, 25.78, 26.00, 26.64, 27.88, and 28.36 m are all represented as darker quasi horizontal layers in the raw OPTV log (Figure 4a) and as local increases in the gravimetric (Figure 4b) and OPTV-derived (Figure 4c) density data. However, despite depth matching, peaks and troughs in the gravimetrically measured density data do not match up precisely with those in the OPTV-reconstructed density data ($R^2 = 0.32$). This weak match between measured density and reconstructed density at the scale of 10^{-3} – 10^{-2} m can be explained by a combination of several possible influences, considered below.

[16] 1. The measured data are subject to an empirically determined error, defined as one standard deviation in sample pairs recovered from the same depth, of up to 4% (section 2.2.2). This alone could account for a density variation of ~ 55 kg m⁻³ for this data set. However, the general match between the overall gravimetric- and OPTV-derived density profiles suggests that the actual error in measured density is less than this and that this effect is supplemented by other factors.

[17] 2. OPTV-derived density is laterally averaged at the scale of the borehole cross section, but material density is inhomogeneous at this scale. None of the darker subhorizontal layers in the raw OPTV log shown in Figure 4a are precisely uniform around the full borehole circumference, indicating lateral variability at the scale of millimeters to centimeters. For example, the thin dark layer at 25.78 m is present only in the SW quadrant of the borehole. This particular mismatch between the reconstructed OPTV density of 683 kg m⁻³ (Figure 4c) and the gravimetrically measured density of

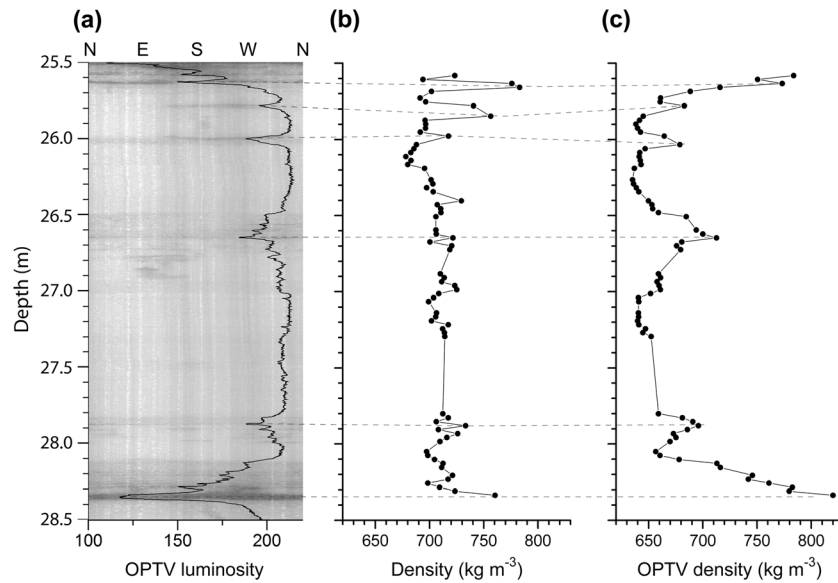


Figure 4. Expansion of RBIS data between 25.5 and 28.5 m depth: (a) raw OPTV log with overlaid luminosity trace, (b) gravimetric density measured on samples of dimension ~ 26 mm from four core sections, and (c) density reconstructed from OPTV luminosity (equation (2)) subsampled at the same scale as the gravimetrically measured density samples shown in Figure 4b. Superimposed dashed lines join likely ice-rich/high-density layers across the three records.

756 kg m⁻³ (Figure 4b) could therefore be due to the (26 mm dimension) gravimetric sample being cut from this relatively dense part of the core while the OPTV data are averaged across the complete borehole circumference. Indeed, the darkest 26×26 mm area of the raw OPTV image at this depth has a mean pixel luminosity of 172, yielding, through equation (2), an OPTV density of 772 kg m⁻³. This is 89 kg m⁻³ higher than the OPTV density reconstructed from the horizontally averaged luminosity and 16 kg m⁻³ higher than that measured gravimetrically. All of the observed difference between measured firm density and OPTV-derived density at this depth can therefore be accounted for by centimeter-scale lateral variations in the former.

[18] 3. The OPTV probe records light reflected from the borehole's walls following emission from a ring of LEDs located ~ 80 mm above the hyperboloidal mirror (section 2.2.1). Therefore, depending on the precise reflective properties of the section of borehole wall being logged, the recorded signal may not have come precisely from the horizontal plane given by the midpoint between the LED array and mirror. Although this effect is unlikely to result in any notable offset, it could blur layer boundaries that are, in reality, sharp.

[19] 4. The two data sets could still be offset, at least by some millimeters, as a consequence of imperfect depth matching and depth control, particularly in the core depth.

3. Summary and Discussion

[20] OPTV luminosity traces from two boreholes drilled in the area of the Roi Baudouin Ice Shelf, Antarctica, have been compared with material density measured directly on snow, firm and ice sampled from the corresponding cores. At the scale of each borehole (~ 67 and 118 m) and below the grain boundary sliding to sintering transition (here found to be ~ 5 and ~ 7 m deep), material density increases down-core and OPTV luminosity decreases down borehole. Plotting density directly against luminosity reveals that the former varies as

an exponential function of the latter and that this relationship (equation (2)) holds for the two boreholes investigated, both individually and combined. Best fit regression statistics indicate that the combined match yields an R^2 value of 0.96, strongly suggesting that OPTV luminosity provides a close proxy for material density.

[21] Evaluation of the global applicability of this relationship requires further data from locations with more diverse densification processes. Nonetheless, the two ice shelf sites analyzed herein are characterized by markedly different concentrations of infiltration ice (Figure 2) and accumulation rates (section 2.3.1), encompassing much of the variability anticipated at Antarctic ice shelves. Whether equation (2) also holds for boreholes drilled by hot water remains to be evaluated, but one would anticipate that a separate calibration would be needed to account for the refreezing of drill water lost to permeable borehole walls.

[22] Equation (2) may also hold for the densification of ice, albeit with a lower degree of statistical explanation ($R^2 = 0.32$). We provisionally attribute this decrease in reflectivity with increasing ice density to reflective air bubbles trapped within the ice becoming both smaller and more spherical with depth [e.g., *Ueltzhöffer et al.*, 2010].

[23] **Acknowledgments.** We thank the International Polar Foundation for logistical support and the Belgian Science Policy Office (BELSPO) and NERC (grant NE/J013544/1) for financial support. TM was supported by a Knowledge Enterprise Skills Scholarship and BH by the Climate Change Consortium of Wales.

[24] The Editor thanks Elizabeth Morris and an anonymous reviewer for their assistance in evaluating this manuscript.

References

- Alley, R. B., C. R. Bentley, and J. H. Porepezko (1987), Grain-growth in unstrained glacial ice, *J. Phys.*, 48(C-1), 659–660.
- Bramall, N. E., R. C. Bay, K. Woschnagg, R. A. Rohde, and P. B. Price (2005), A deep high-resolution optical log of dust, ash, and stratigraphy

- in South Pole glacial ice, *Geophys. Res. Lett.*, 32, L21815, doi:10.1029/2005GL024236.
- Breton, D. J., G. S. Hamilton, and C. T. Hess (2009), Design, optimization and calibration of an automated density gauge for firn and ice cores, *J. Glaciol.*, 55(194), 1092–1100.
- Fudge, T. J., and B. E. Smith (2010), Light propagation in firn: Application to borehole video, *J. Glaciol.*, 56(198), 614–624.
- Gerland, S., H. Oerter, J. Kipfstuhl, F. Wilhelms, H. Miller, and W. D. Miners (1999), Density log of a 181 m long ice core from Berkner Island, Antarctica, *Ann. Glaciol.*, 29(1), 215–219.
- Hawley, R. L., and E. M. Morris (2006), Borehole optical stratigraphy and neutron-scattering density measurements at Summit, Greenland, *J. Glaciol.*, 52(179), 491–496.
- Hubbard, B., and T. Malone (2013), Optical-televviewer-based logging of the uppermost 630 m of the NEEM deep ice borehole, Greenland, *Ann. Glaciol.*, 54(64), 83–89.
- Hubbard, B., S. Roberson, D. Samyn, and D. Merton-Lyn (2008), Digital optical televiewing of ice boreholes, *J. Glaciol.*, 54(188), 1–8.
- Hubbard, B., J. L. Tison, F. Pattyn, M. Dierckx, T. Boereboom, and D. Samyn (2012), Optical-televviewer-based identification and characterization of material facies associated with an Antarctic ice-shelf rift, *Ann. Glaciol.*, 53(60), 137–146.
- Malone, T., B. Hubbard, D. Merton-Lyn, P. Worthington, and R. Zwiggelaar (2013), Borehole and Ice Feature Annotation Tool (BIFAT): A program for the automatic and manual annotation of glacier borehole images, *Comput. Geosci.*, 51, 381–389.
- Morris, E. M., and J. D. Cooper (2003), Instruments and methods. Density measurements in ice boreholes using neutron scattering, *J. Glaciol.*, 49(167), 599–604.
- Sjögren, B., O. Brandt, C. Nuth, E. Isaksson, V. Pohjola, J. Kohler, and R. S. W. Van De Wal (2007), Determination of firn density in ice cores using image analysis, *J. Glaciol.*, 53(182), 413–419.
- Ueltzhöffer, K. J., V. Bendel, J. Freitag, S. Kipfstuhl, D. Wagenbach, S. H. Faria, and C. S. Garbe (2010), Distribution of air bubbles in the EDML and EDC (Antarctica) ice cores, using a new method of automatic image analysis, *J. Glaciol.*, 56(196), 339–348.